

Nonlinear relationship between signal and gas concentration in high-precision off-axis integrated cavity output spectroscopy

Xinxin Wei(韦欣欣), Biao Ye(叶标), Yi Jiao(焦一), Xin Meng(孟鑫), and Jingjing Wang(王静静)
Citation: Chin. Phys. B, 2026, 35 (**3**): 034206. DOI: 10.1088/1674-1056/adfa79
http://cpb.iphy.ac.cn; http://iopscience.iop.org/cpb

What follows is a list of articles you may be interested in

Simultaneous detection of CH_4 and CO_2 through dual modulation off-axis integrated cavity output spectroscopy

Yi-Xuan Liu(刘艺璇), Zhou-Bing Wang(王周兵), Xin-Xin Wei(韦欣欣), Jing-Jing Wang(王静静), Xin Meng(孟鑫), and Gui-Lin Mao(毛桂林)
Chin. Phys. B, 2023, 32 (**10**): 104209. DOI: 10.1088/1674-1056/acdac1

Creation mechanism of electron-positron pair on equally spaced multiple localized fields

Chuan-Ke Li(李传可), Nan-Sheng Lin(林南省), Xian-Xian Zhou(周鲜鲜),Miao Jiang(江淼), and Ying-Jun Li(李英骏)
Chin. Phys. B, 2023, 32 (**9**): 094202. DOI: 10.1088/1674-1056/acd7cd

Absorption linewidth inversion with wavelength modulation spectroscopy

Yue Yan(颜悦), Zhenhui Du(杜振辉), Jinyi Li(李金义), Ruixue Wang(王瑞雪)
Chin. Phys. B, 2018, 27 (**2**): 024205. DOI: 10.1088/1674-1056/27/2/024205

Wavelength modulation spectroscopy for measurements of gas parameters in combustion field

Dong-Sheng Qu(屈东胜), Yan-Ji Hong(洪延姬), Guang-Yu Wang(王广宇), Hu Pan(潘虎)
Chin. Phys. B, 2017, 26 (**6**): 064207. DOI: 10.1088/1674-1056/26/6/064207

Measurements of atmospheric NO_3 radicals in Hefei using LED-based long path differential optical absorption spectroscopy

Xue Lu(卢雪), Min Qin(秦敏), Pin-Hua Xie(谢品华), Jun Duan(段俊), Wu Fang(方武), Liu-Yi Ling(凌六一), Lan-Lan Shen(沈兰兰), Jian-Guo Liu(刘建国), Wen-Qing Liu(刘文清)
Chin. Phys. B, 2016, 25 (**2**): 024210. DOI: 10.1088/1674-1056/25/2/024210

Nonlinear relationship between signal and gas concentration in high-precision off-axis integrated cavity output spectroscopy

Xinxin Wei(韦欣欣), Biao Ye(叶标), Yi Jiao(焦一), Xin Meng(孟鑫), and Jingjing Wang(王静静)†

School of Physics and Electronic Engineering, Jiangsu Normal University, Xuzhou 221116, *China*

(Received 20 May 2025; revised manuscript received 25 July 2025; accepted manuscript online 12 August 2025)

Off-axis integrated cavity output spectroscopy (OA-ICOS) is an extremely sensitive technique for measuring trace gas concentrations. Nevertheless, recent research has indicated that when the reflectivity of the mirrors forming the cavity is excessively high, it affects the linearity between the absorption signal and concentration. In this study, the causes and limitations of this phenomenon are discussed based on the Beer–Lambert law and the law of light propagation within the cavity. A new equation is derived to describe the nonlinear relationship between the integral area of absorption spectra and gas concentration. The absorption spectra of CO_2 and CH_4, measured under different experimental conditions and concentrations, were fitted with Voigt functions to obtain parameters such as peak values and integral areas, which were used to verify the theoretical derivation process and results. The experimental results demonstrate that the relationship between the area of the measured absorption spectra and the gas concentration is consistent with the new formula, with an average fitting correlation coefficient of 0.9998. Meanwhile, the experimental results also demonstrate that the effective optical path length indeed decreases with increasing concentration. Furthermore, the cavity reflectances (99.99644% at 6242.6 cm^{-1} and 99.99833% at 6046.96 cm^{-1}) derived from the fitting coefficient of the new concentration expression closely match the reflectances (99.99727% at 6242.6 cm^{-1} and 99.99868% at 6046.96 cm^{-1}) obtained by applying the classical formula to the spectra of the lowest gas concentration. These experimental results validate the theoretical deduction process and expression. This research provides insights for the theoretical and practical advancements of OA-ICOS, which is significant for advancing high-precision trace gas detection technology.

Keywords: integrated cavity output spectroscopy, trace gas concentration, mirrors reflectivity, nonlinear relationship, Beer–Lambert law

PACS: 42.68.Ca, 07.88.+y, 42.62.Fi, 95.85.Jq

DOI: 10.1088/1674-1056/adfa79 **CSTR:** 32038.14.CPB.adfa79

1. Introduction

Off-axis integrated cavity output spectroscopy (OA-ICOS) is a technology that injects a specific wavelength laser off-axis into an optical cavity, thereby increasing the optical signal.[1–3] The multiple reflections of light inside the cavity increase the interaction time between the light and the sample, effectively extending the optical path length and allowing for qualitative or quantitative analysis based on the output spectra. The optical resonant cavity enhances the effective optical path length, adhering to the Beer–Lambert law, which states that substance concentration is proportional to the optical path length, the peak intensity of the absorption spectra, and the integral area. Light can reflect thousands of times between the two high-reflectivity mirrors, extending the effective optical path length to 1 km–30 km. This technique, therefore, offers high detection sensitivity. Additionally, off-axis incidence effectively suppresses cavity noise, simplifies cavity adjustment, and reduces stability requirements, making it widely used for trace gas detection.[4–11]

In 2001, Baer utilized OA-ICOS to measure mixing ratios in the air, and Engel *et al.* applied it for real-time monitoring of climate change.[6] Subsequently, with the efforts of a large number of researchers, OA-ICOS technology has undergone rapid development.Clouser *et al.*[7] introduced asymmetric optical components in an instrument based on off-axis integration cavity output spectra, overcoming the constraint effect of optical skewness in the OA-ICOS cavity and significantly improving the collection of emitted light. Kaiyuan Zheng *et al.* proposed a near-infrared ultra-compact cage OA-ICOS measurement system, achieving high sensitivity and precision detection of C_2H_2 using a wavelength modulation spectroscopy (WMS) measurement scheme.[8] In 2021, Wang developed a prototype for in situ measurement of CO_2 and CH_4 concentrations based on the Dual-OA-ICOS system.[9] OA-ICOS technology has also become the preferred method for high-sensitivity isotope gas detection.[10,11] For example, Han used OA-ICOS to measure the direct absorption and second harmonic signals of three CO_2 isotopes ($^{16}O^{12}C^{16}O$, $^{16}O^{13}C^{16}O$, and $^{16}O^{12}C^{18}O$).[10]

In 2019, Tian[12] measured CH_4 using an OA-ICOS system equipped with 99.999% reflectivity mirrors and a laser component with a central wavelength of 1653 nm. He explored the linear relationship between the integral area and concentration in two concentration ranges. Under the ex-

†Corresponding author. E-mail: jjwang@jsnu.edu.cn

© 2026 Chinese Physical Society and IOP Publishing Ltd. All rights, including for text and data mining, AI training, and similar technologies, are reserved.

perimental condition of 40.53 kPa, he found that the slopes for integral area versus CH_4 concentration were 0.03 for the 0.2 ppmv–1.4 ppmv range and 0.0001 for the 40 ppmv–180 ppmv range, indicating a nonlinear relationship between integral area and concentration in the larger concentration range (0.2 ppmV–180 ppmv). Wang[13] obtained similar results in an in situ dissolved gas measurement study using OA-ICOS, where CH_4 showed a nonlinear relationship with the integral area in a range of 0 ppmv–10 ppmv, and CO_2 in a range of 0 ppmv–2000 ppmv. Wang *et al.*[14] investigated large dynamic concentration range measurements under nonlinear conditions, showing that at low gas concentrations, there was a good linear relationship between transmitted light intensity and gas concentration at different positions away from the absorption peak. However, in non-weak absorption conditions, this relationship did not hold. Overall, in high-precision OA-ICOS systems, the classical linear relationship between spectral signals and gas concentration does not suffice when the gas concentration range is large. Therefore, if the classical linear relationship is still used to process high-precision OA-ICOS system signals, it can only accurately measure gas concentration within a very narrow concentration range. It is necessary to study this nonlinear relationship in high-precision OA-ICOS systems.

This study investigates the nonlinear relationship between gas concentration and absorption signals in high-precision OA-ICOS systems. Based on the Beer–Lambert law and the propagation law of light in a cavity, we theoretically explore this nonlinear relationship and establish a new equation relating gas concentration to the integral area. We verify our theoretical derivation by measuring the absorption spectra of CO_2 and CH_4 standard gases under different temperatures and pressures.

2. Theoretical analysis

According to the Beer–Lambert law, when a laser beam with an initial intensity I_0 and frequency v propagates through an absorbing medium of thickness L, a portion of the light energy is absorbed by the medium, thereby reducing the intensity of the light emitted. In the context of spectroscopic measurements, the general absorption light can be expressed as follows:[15,16]

$$\Delta I(v) = \alpha(v)L = -\ln\left(\frac{I}{I_0}\right) = N\sigma(v)L = NS\chi(v)L, \quad (1)$$

where $\alpha(v)$ is the absorption coefficient (in unit cm^{-1}), I is the intensity of the light after passing through the medium, $\sigma(v)$ is the absorption cross-section (in units cm^2/molecule), N is the molecular number density (in units molecule/cm^3), S is the spectral absorption line intensity (in units cm^{-1}/(molecule cm^{-2})), and $\chi(v)$ is the normalized spectral absorption line shape. According to the above equation, the absorption integral area (A_I) of the spectra can be expressed as follows:

$$A_\mathrm{I} = \int \Delta I(v)\,\mathrm{d}v = NSL\int \chi(v)\,\mathrm{d}v = NSL. \quad (2)$$

In OA-ICOS, the primary losses arise from absorption exhibited by the medium within the cavity and incomplete reflection by the highly reflective mirrors.[17] Let $\alpha(\upsilon)$ be the absorption coefficient, the reflectivity of the two mirrors be $r_1 = r_2 = R$, and the transmissivity be $T = 1-R$. Then, the one-way loss is $\delta = 1-R+\alpha(v)d$ where d denotes the thickness of the absorbing material. The decay time constant (cavity ring-down time), which corresponds to the time required for the initial intensity to decay to 1/e, is given by

$$\tau = \frac{d}{c(1-R+\alpha(v)d)}. \quad (3)$$

The ring-down time τ depends on the reflectivity and length of the cavity, as well as the absorption properties of the medium within the cavity, and is independent of the laser pulse intensity. In the absence of an absorbing or scattering medium in the cavity, τ is

$$\tau = \frac{d}{c(1-R)}. \quad (4)$$

Generally, the loss caused by single-pass absorption ($\alpha(v)d$) is much smaller than that of a single-pass mirror's loss ($1-R$). That is, when the weak absorption condition $1-R \gg \alpha(v)d$ is satisfied, the influence of $\alpha(v)d$ on the cavity ring-down time τ is relatively insignificant. The effective optical path length is thus expressed as follows:[15–17]

$$L = c\tau = \frac{d}{1-R}. \quad (5)$$

For a selected optical resonant cavity, the reflectivity in the specified band should remain constant and not vary with parameters such as gas concentration and pressure. Calculating the gas concentration by substituting L into Eq. (2) which demonstrates a linear relationship between concentration, peak intensity, and the integral area of the absorption spectra.

If the one-way loss does not satisfy the weak absorption condition $1-R \gg \alpha(v)d$, then the effective optical path length should be calculated using Eq. (3)

$$L = c\tau = \frac{d}{1-R+\alpha(v)d}. \quad (6)$$

This equation indicates that the effective optical path will decrease as the absorption coefficient increases. Substituting this into Eq. (2) yields a new equation

$$A_\mathrm{I} = \frac{NSd}{1-R+N\sigma(v)d}. \quad (7)$$

This equation indicates that when we take the single-pass absorption loss of the gas into account to calculate the effective optical path, the gas concentration is no longer linearly related to the peak intensity and the integral area of the absorption spectra. By further manipulating the above equation, obtain the expression formula for N as

$$N = \frac{1-R}{d}\frac{A_{\mathrm{I}}}{S-\sigma(v)A_{\mathrm{I}}} = \frac{1-R}{Sd}\frac{A_{\mathrm{I}}}{1-\chi(v)A_{\mathrm{I}}}, \tag{8}$$

where $\sigma(v)/S = \chi(v)$ is the normalized spectral absorption line shape function, where the specific formulation depends on factors such as temperature (T), pressure (P), laser linewidth, and instrument response bandwidth during measurement. In practical application, the unit of gas concentration is usually the volume ratio. For example, the total volume of N_2 and CO_2 mixed gas is V_0, where the volume of CO_2 is V_{C}, the volume of N_2 is V_{N}, and the concentration of CO_2 can be described as $C = V_{\mathrm{C}}/V_0$. The gas volume ratio is equal to the ratio of molecular number density, that is, the volume ratio concentration $C = N/N_{\mathrm{T}}$, N_{T} is the total gas molecular density. Let N_{L} be the total gas molecular density under standard environment ($p_0 = 273.15$ K, $t_0 = 101.325$ kPa $= 760$ Torr, 1 Torr $= 1.33322\times10^2$ Pa), P be the actual pressure, T be the actual temperature, and N_{T} can be deduced as $N_{\mathrm{T}} = N_{\mathrm{L}}PT_0/P_0T$. Substituting this into Eq. (8), we obtain

$$\begin{aligned} C &= \frac{N}{N_{\mathrm{T}}} = \frac{1-R}{Sd}\frac{A_{\mathrm{I}}}{1-\chi(v)A_{\mathrm{I}}}\frac{P_0T}{N_{\mathrm{L}}PT_0} \\ &= K_0\frac{T(1-R)}{PSd}\frac{A_{\mathrm{I}}}{1-\chi(v)A_{\mathrm{I}}}, \end{aligned} \tag{9}$$

where $K_0 = P_0/N_{\mathrm{L}}T_0 = 1.03556\times10^{-19}$ (cm^3·k^{-1}·Torr). In practical measurements, R is the reflectivity of the mirrors that constitute the resonant cavity, and the manufacturers generally provide a reference value range. d is the distance between the reflecting surfaces of the two mirrors, which can be measured. The gas pressure and temperature in the cavity can also be easily measured. The integral area A_{I} of the measured absorption spectra can be acquired through peak fitting. At the same time, S represents the absorption line intensity of the gas under specified wavelength and temperature conditions, which can be retrieved from the HITRAN database. In general, we can verify Eq. (9) through experiments. We prepared several sets of CO_2 and CH_4 standard gases at varying concentrations. We measured their absorption spectra to investigate the relationship between gas concentration, effective optical path length, intensity of absorption spectral signals, and integral area, thereby validating the theoretical analysis.

3. Experimental scheme

3.1. Experimental setup and system configuration

The optical measurement system, as shown in Fig. 1, comprises individual sections for laser modulation, gas measurement, signal acquisition and processing, and pressure and temperature monitoring. In this system, the laser controller (SRS, LDC501) manages the temperature and current of the laser diodes (NEL, 1603 nm and 1653 nm). The signal generator (REGOL, DG1062) sends triangular wave scanning signals and trigger signals to the laser controller and signal acquisition card (NI, USB-6210), respectively. A custom-built photoelectric detector converts optical signals into electrical signals, which are collected by a LabVIEW program via the signal acquisition card. Optical components are connected using cage structure mounting rods for integrated alignment along the cavity axis. The laser beam is collimated using a collimator and aligned with the incident window of the cavity using a four-dimensional tuning frame. The collimator adjusts the divergence angle and the position of the beam waist to perfectly match the mode of the resonant cavity. At the other end of the cavity, a cage structure is used to connect the short focusing mirrors, filter, and photoelectric detector. The filter, a Thorlabs 25-mm-diameter long-wavelength filter with a starting wavelength of 1500 nm, protects the spectral signals received by the photoelectric detector from ambient light.

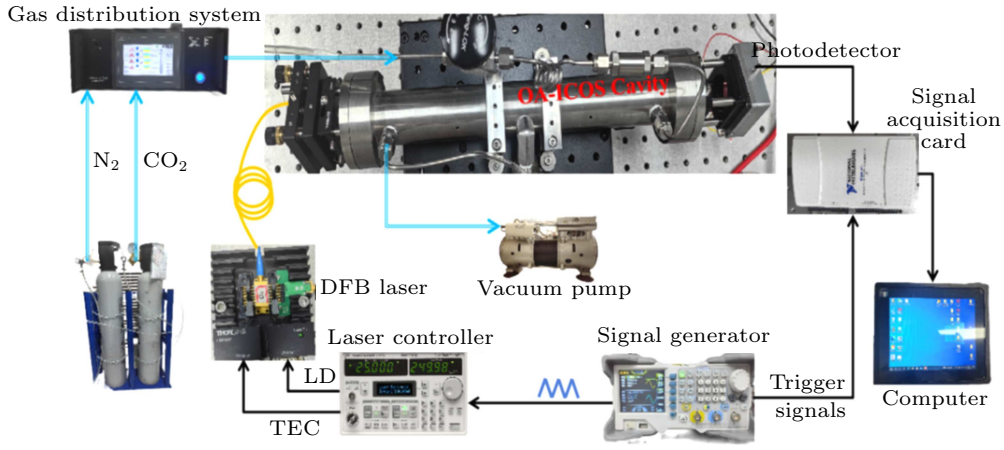


Fig. 1. Schematic diagram of the OA-ICOS system.

The optical resonant cavity consisted of two high-reflective mirrors with a curvature radius of 1 m and a reflectivity of 99.999%, spaced approximately 28 cm apart. The one-way loss of cavity mirrors is $1-R=10^{-5}$. Using the HITRAN database, under experimental conditions of 25 °C and 150 Torr, the theoretical absorption coefficient of 100 ppmv (*i.e.*, 1.0×10^{-4}) CO_2 at 6242.67211 cm^{-1} is approximately 5.715×10^{-7} cm^{-1}, and the calculated one-way absorption loss is $\alpha(v)d=3.4\times10^{-6}$; the absorption coefficient of 2×10^{-6} CH_4 at 6046.96 cm^{-1} is 4.2×10^{-7} cm^{-1}, one way absorption loss is 1.18×10^{-5}. These values indicate that the one-way absorption loss is very close to the one-way cavity mirror loss, no longer meeting the weak absorption conditions. Such an experimental setup meets the requirements for the next stage of research. These concentrations served as a boundary for the weak absorption limits of CO_2 and CH_4 in this experimental system, providing a basis for further validation and verification.

3.2. Sample conditioning and environmental parameter design

Using a gas distribution system (customized with full-scale accuracy of 0.2%, and reading accuracy of 1%), 5.08×10^{-3} CO_2 and 5.0×10^{-5} CH_4 standard gases were mixed with N_2 at different flow rate ratios, thereby preparing two sets of CO_2 and CH_4 standard gases. Thirty different concentrations of CO_2, ranging from 0 to 5.08×10^{-3}, were prepared and then tested at various temperatures (including 23.2 °C and 27.3 °C) and three different pressures (60 Torr, 82.5 Torr, and 105 Torr). Twelve different concentrations of CH_4, ranging from 0 to 50 ppmv were prepared and then tested at temperatures of 21.1 °C and three different pressures (53 Torr, 75 Torr, 98 Torr). Table 1 lists the gas concentration used in the following experiments. For the convenience of data calculation and uniform plotting standards, gas units in subsequent articles are expressed in volume ratios, where one ppmv is equivalent to 1×10^{-6}.

Table 1. Concentrations of CO_2 and CH_4.

	Concentration (10^{-6})									
Weak absorption of CO_2	10	20	30	40	50	60	70	80	90	100
Strong absorption of CO_2	115	156	198	241	285	330	425	526	633	747
	869	1000	1222	1677	2159	2671	3215	3796	4416	5080
Weak absorption of CH_4	0.3	0.5	0.82	1.27	1.74	2				
Strong absorption of CH_4	3.77	12.2	21.1	31.5	43.2	50				

4. Results and discussion

4.1. The absorption spectra of CO_2 and CH_4

We collected the absorption spectra of various concentrations of CO_2 and CH_4 at different temperatures and pressures, as shown in Table 1. Figure 2 presents the absorption spectra of a group of CO_2 and CH_4. As clearly shown, the peaks of CO_2 and CH_4 continue to rise as their concentrations increase. To conduct further analysis of the experimental data, the absorption spectrum was then fitted using the Voigt function to obtain the peak intensity and integral area, which will serve as the fundamental basis for subsequent data analysis.

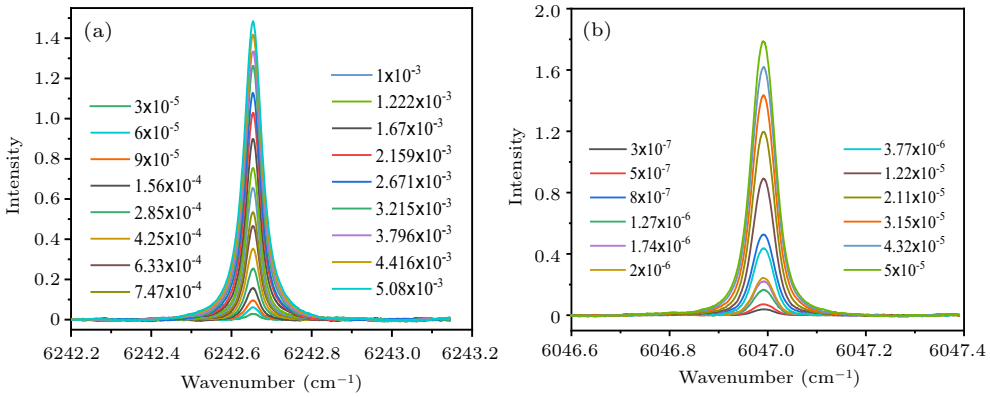


Fig. 2. (a) Partial spectra of CO_2 at 23.2 °C, 105-Torr experimental conditions; (b) spectra of CH_4 at 23.2 °C, 60-Torr experimental conditions.

The fitting results of the absorption spectra of 6×10^{-5} CO_2 and 5×10^{-7} CH_4 using the Voigt function are illustrated in Fig. 3. It is evident that the residual distribution between the CO_2 absorption spectrum and the Voigt fitting curve is relatively uniform, with a smaller amplitude. In contrast, the residual distribution of CH_4 exhibits significant fluctuations, particularly with larger amplitudes near the absorption peak, featuring prominent maxima and minima. The reason is that the absorption spectrum of CH_4 in this region is comprised of three closely spaced absorption lines, rendering the spectrum

imperfectly aligned with the Voigt function.

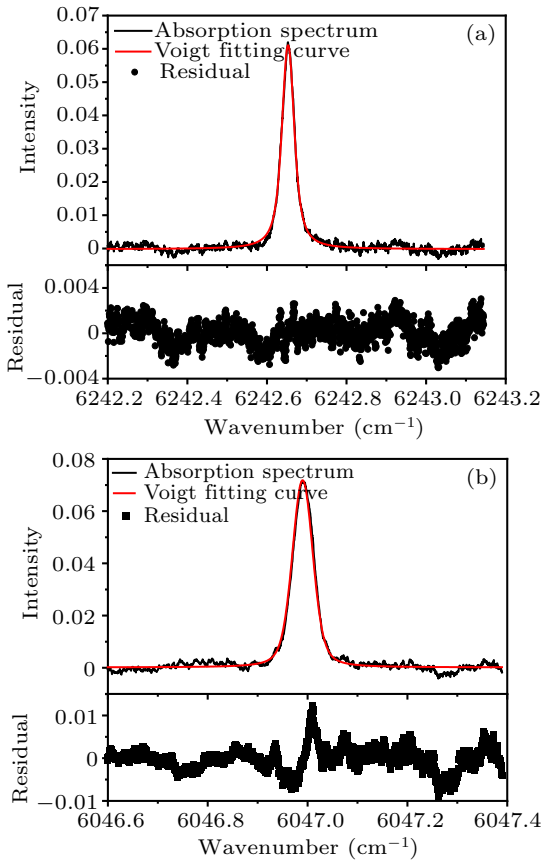


Fig. 3. (a) Fitting effect of the Voigt function for 6×10^{-5} CO_2 absorption spectrum at 23.2 °C, 105 Torr; (b) fitting effect of the Voigt function for 5×10^{-7} CH_4 absorption spectrum at 23.2 °C, 60 Torr.

After the Voigt fitting, the peak value of the 6×10^{-5} CO_2 absorption spectrum is 0.062, and the standard deviation (SD) of the residual is 0.00108. Further calculations indicate that the signal-to-noise ratio (SNR) of the spectral signal is 18.3, and the 2σ value is 6.56×10^{-6}, which represents the minimum detectable limit for measuring CO_2. After the Voigt fitting, the peak value of the 5×10^{-7} CH_4 absorption spectrum was 0.072, and the residual SD was 0.00232. SNR of the spectral signal is 31, and the 2σ value is 3.22×10^{-8}, which is the minimum detection limit of CH_4 measured by the system.

4.2. Relationship between absorption spectra intensity and gas concentration across different ranges

Figure 4 shows the relationship between CO_2 peak intensity and concentration under six different temperature and pressure conditions. As shown in Figs. 4(a) and 4(c), irrespective of experimental conditions, CO_2 concentrations within the 0–1.0×10^{-4} range exhibit a significant linear relationship with peak intensity. Linear fitting of the weak peak intensity of absorption spectra and concentration for six groups yielded coefficients of fit correlation (R^2) ranging from 0.99856 to 0.99949. Overall, within this concentration range, the peak intensity of the absorption spectra maintains a significant linear relationship with the concentration. However, when the concentration range extends to 5.08×10^{-3}, the spectral peak intensity exhibits a significant nonlinear relationship with the concentration.

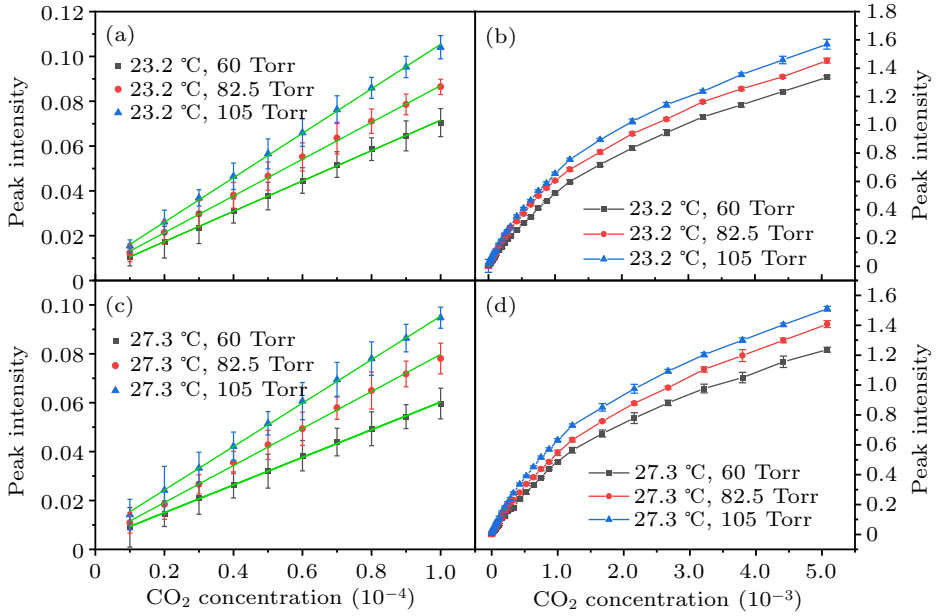


Fig. 4. Relationship between absorption peak intensity and gas concentration under different temperatures and pressures of CO_2: (a) 23.2 °C and various pressures within the range of 3×10^{-5}–1×10^{-4}; (b) 23.2 °C and various pressures within the range of 3×10^{-5}–5.08×10^{-3}; (c) 27.3 °C and various pressures within the range of 3×10^{-5}–1×10^{-4}; (d) 27.3 °C and various pressures within the range of 3×10^{-5}–5.08×10^{-3}.

For the same data processing procedure of CH_4 gas, the relationship between its concentration and peak value is obtained and shown in Fig. 5. Similar to Fig. 4 that the relationship is also nonlinear in the high concentration range (3×10^{-7}–5×10^{-5}) and linear in the low concentration range (3×10^{-7}–2×10^{-6}). Overall, the peak values of the absorption spectra of CO_2 and CH_4 show consistency with the change in concentration. As the concentration increases, the slope between the in-

tensity of the absorption peak and the concentration decreases; that is, the growth rate of the absorption peak decreases with increasing concentration. This result also indicates that this nonlinear relationship exists not only in CO_2 gas but also in other gases.

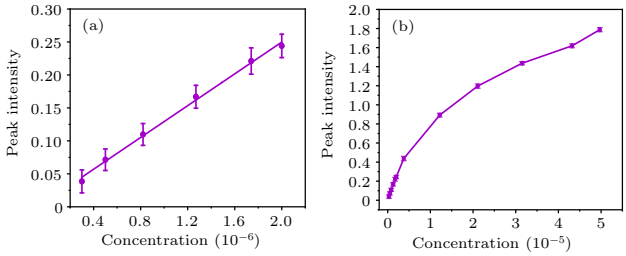


Fig. 5. The relationship between the peak intensity of 3×10^{-7}–5×10^{-5} CH_4 at 21.1 °C and 60 Torr and its concentration.

In light of the theoretical analysis in Section 2, this experimental result is quite reasonable. At higher concentrations, the one-way absorption loss increases, no longer meeting the conditions for weak absorption. The effective optical path follows the variation law of formula (6). As the concentration increases, the effective optical path length gradually decreases, and the growth rate of the absorption spectral intensity decreases with increasing concentration (as shown in Eq. (1)).

4.3. Relationship between integral area and gas concentration across different ranges

The relationship between integral area and CO_2 concentration under six experimental conditions is illustrated in Fig. 6. As shown in Figs. 6(a) and 6(c), within the concentration range of 0–1.0×10^{-4}, the integral area and concentration exhibit a significant linear relationship. Conversely, figures 6(b) and 6(d) demonstrate that within the range of 0–5.080×10^{-3}, the integral area and concentration exhibit a significant nonlinear relationship. The slope representing the relationship between the concentration (Y-axis) and the integral area (X-axis) is increasing, indicating that the growth rate of the integral area decelerates as the gas concentration rises.

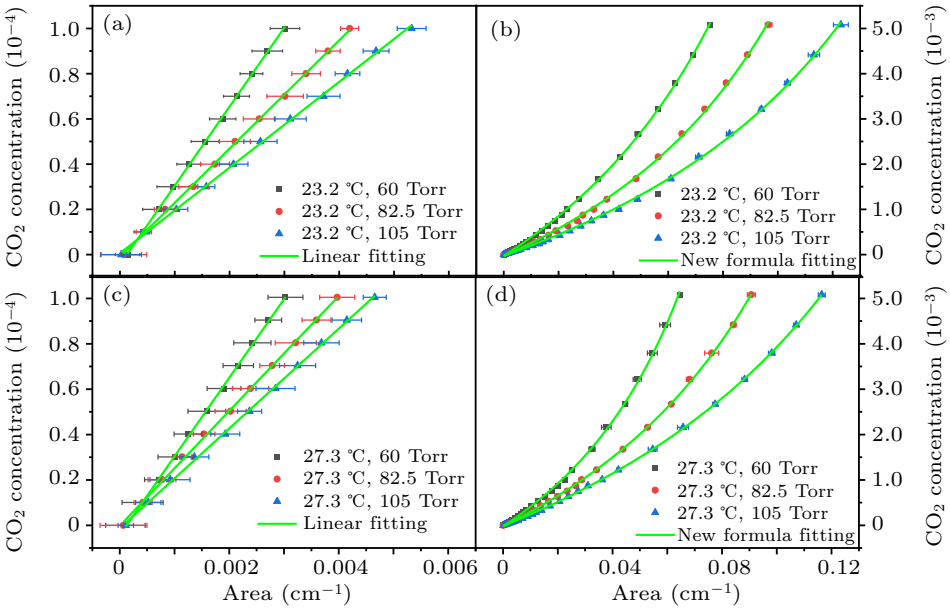


Fig. 6. Relationship between CO_2 integral area and gas concentration under different temperatures and pressures: (a) 23.2 °C and various pressures within the range of 0–1×10^{-4}; (b) 23.2 °C and various pressures within the range of 0–5.08×10^{-3}; (c) 27.3 °C and various pressures within the range of 0–1×10^{-4}; (d) 27.3 °C and various pressures within the range of 5.08×10^{-3}.

The relationship between CH_4 concentration and integral area under three pressure conditions at 21.1 °C is shown in Fig. 7. It is very similar to the result of CO_2 in Fig. 6. Within the range of 0–2×10^{-6}, CH_4 concentration and integral area show a linear relationship. When the concentration range expands to 5.0×10^{-5}, the relationship between the two becomes significantly non-linear. This result eliminates the influence of the accidental factor of the non-linearity of CO_2 itself. The reason for this experimental phenomenon is that as the effective optical path decreases with increasing concentration (will be proved in the next section), the ratio between the integral area and concentration decreases (as shown in Eq. (2)), that is, the growth rate of the integral area decelerates with increasing concentration.

To facilitate the subsequent processing of experimental data, let $A=\chi(v)$ and $B=K_0\frac{T(1-R)}{PSd}$ simplify Eq. (9) to

$$y=\frac{Bx+C_0}{1-Ax}, \tag{10}$$

where C_0 is a constant accounting for measurement error, the experimental data were curve-fitted according to Eq. (10) (green curves in Figs. 6(b) and 6(d), purple curve in Fig. 7(b)). As shown in Figs. 6 and 7, the trend of the integral area increasing with concentration under different pressure and temperature conditions follows the curve described by formula (10). The specific parameters obtained by curve fitting are shown in Table 2.

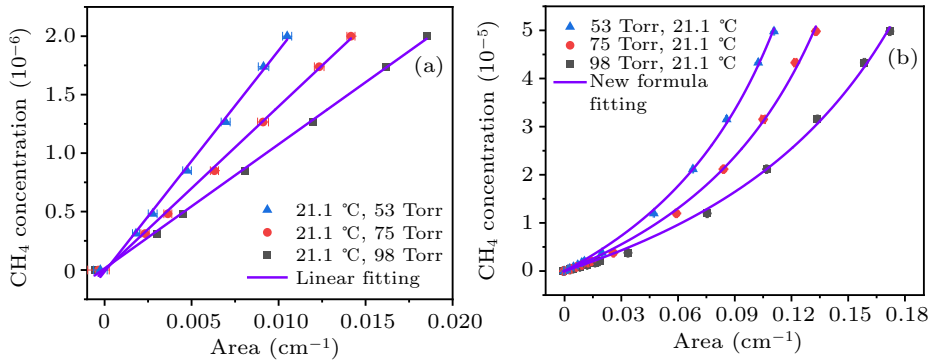


Fig. 7. The relationship between CH_4 integral area and gas concentration under different pressures: (a) 21.1 °C and various pressures within the range of 0–2×10^{-6}, (b) 21.1 °C and various pressures within the range of 0–5×10^{-5}.

Table 2. Relevant fitting parameters of different gases under various temperatures and pressures based on the nonlinear concentration inversion formula.

Gas	Temperature (°C)	Pressure (Torr)	Coefficient A	Coefficient B	R^2
CO_2	23.2	60	5.67790	0.03933	0.99982
	23.2	82.5	5.07954	0.02749	0.99969
	23.2	105	3.95879	0.02165	0.99976
	27.3	60	7.78054	0.04012	0.9997
	27.3	82.5	5.12324	0.03032	0.99988
	27.3	105	3.77027	0.02461	0.99996
CH_4	21.1	53	4.80773	2.15194×10^{-4}	0.99972
	21.1	75	4.28297	1.67159×10^{-4}	0.99945
	21.1	98	3.18359	1.35512×10^{-4}	0.99950

The coefficients of determination (R^2) of the regression model range from 0.99969 to 0.99996, with an average of 0.9998. These values indicate that the experimental data are very consistent with Eq. (10), verifying the correctness of the derived formula. The fitting parameters indicate that fitting coefficients A and B increase with rising temperature and decrease with increasing pressure. The value of A, representing the normalized absorption line shape, aligns with the fact that higher pressure broadens the line width of direct absorption spectra. As shown in the expression formula $B = K_0\frac{T(1-R)}{PSd}$, it is directly proportional to temperature and inversely proportional to pressure, which is consistent with experimental measurements indicating that the B value increases with rising temperature and decreases with increasing pressure.

4.4. Effective optical path length and cavity reflectivity

The effective optical path[15,16] $L = \frac{A_1 rT}{N_A PCS}$ can be obtained using the integral area and gas concentration based on Eq. (2), where $N_A = N\frac{rT}{PC}$, $r = 8.31\times10^{-6}$ cm^3·Pa/(k·mol) is the ideal gas constant and related to the unit chosen of temperature and pressure. T (in unit K) and P (in unit Torr) represent the temperature and pressure, respectively, in the experimental conditions. C is the relative volume concentration of the gas (V/V_0, unitless), and S is the intensity of the absorption line of the chosen gas, CO_2 or CH_4. When calculating the effective optical path at any temperature, we retrieved the HITRAN database again to verify the gas absorption line strength S at that temperature.

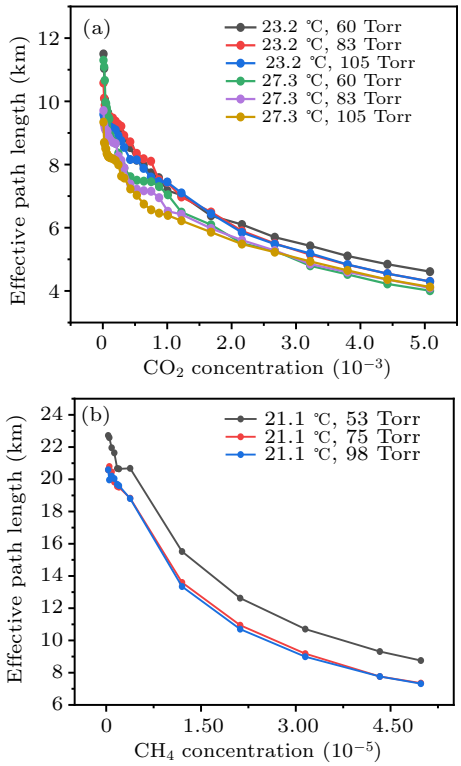


Fig. 8. (a) Relationship of CO_2 concentrations with effective optical path length under different conditions. (b) Relationship of CH_4 concentrations with effective optical path length under different conditions.

The calculated effective optical path under various conditions is illustrated in Fig. 8. Obviously, the concentrations are

inversely proportional to the effective optical path length: as the concentration increases, the effective optical path length decreases, which is in excellent agreement with the conclusions drawn from our previous theoretical analysis (Eq. (6)). The effective optical path of CO_2 decreased from 10.3 km to 4 km (the average value of the six sets of data), with an average effective optical path length of 8 km. The effective optical path of CH_4 decreases from 21 km to 7 km (the average value of the three sets of data), with an average effective optical path of approximately 16 km. When the concentration is very low, the light absorption loss caused by the gas is minimal and can be disregarded, so the effective optical path at this time is long. When the concentration increases, the one-way absorption loss increases substantially, thereby reducing the cavity decay time and effective optical path length. When we substitute the average values of the longest effective optical paths (10.3 km for 1×10^{-5} CO_2 and 12.8 km for 3×10^{-7} CH_4) into formula (5), we can calculate the reflectivity to be 99.99727% and 99.99868%, respectively.

Based on the expression for coefficient B from Eq. (10), derive the calculation formula for $R = 1 - \frac{BPSd}{K_0T}$, where d =28 cm. Then, using this expression and the fitting parameters B, temperature, pressure, and other parameters in Table 3, the reflectivity R can be obtained. When calculating the reflectivity at any temperature, we retrieved the HITRAN database again to verify the gas absorption line strength S at that temperature.

As shown in Table 3, the reflectivity of the cavity mirrors at 6242.67 cm^{-1} ranges from 99.99620% to 99.99660% with an average reflectivity of 99.99644%. The reflectivity range is 99.99821% to 99.99846% at 6046.96 cm^{-1}, with an average reflectivity of 99.99833%. The discrepancy in calculated reflectivity values at different wavelengths arises from the inherent property of dielectric films, which exhibit varying absorption and transmission rates across different wavelength bands. These two reflectivities are very close to those calculated in the previous paragraph using the maximum effective optical path. The primary cause of the discrepancy between the two lies in the relatively significant measurement deviations associated with the weak absorption signal as well as uncertainties in spectral fitting. These reflectivities are lower than the reference reflectivity (99.999%) provided by the manufacturer, due to the mirrors having been contaminated and subsequently cleaned during the early stages of the experiments. Based on our extensive experimental experience, high-reflectivity dielectric films of this grade are highly susceptible to contamination. Once contaminated, regardless of the cleaning method employed, there will be a certain degree of decline in the mirrors' reflectivity. In addition, the inevitable measurement error and other factors in the experiment will also lead to calculation errors in reflectivity.

Table 3. Cavity reflectivity obtained based on the fitting coefficient B.

Wavenumber	Temperature (°C)	Pressure (Torr)	Reflectivity (%)	Average reflectivity (%)
6242.67 cm^{-1}	23.2	60	99.99646	99.99644
	23.2	82.5	99.99660	
	23.2	105	99.99659	
	27.3	60	99.99646	
	27.3	82.5	99.99632	
	27.3	105	99.99620	
6046.96 cm^{-1}	21.1	53	99.99846	99.9983
	21.1	75	99.99831	
	21.1	98	99.99821	

5. Conclusion

This study investigated the nonlinear relationship between gas concentration and absorption spectral signals in a high-precision OA-ICOS system. Confirm from both theoretical and experimental perspectives that when the one-way absorption loss within the cavity is no longer insignificant compared to the one-way cavity mirrors loss, the one-way loss is highly correlated with the gas absorption coefficient (*i.e.*, concentration). Consequently, the decay time and effective optical path of the light traversing the resonant cavity are also linked to the concentration, with increasing concentrations resulting in a reduced effective optical path, which ultimately leads to a clear nonlinear relationship between gas concentration and both the intensity and integral area of the absorption spectrum. A new equation for this nonlinear relationship between concentration and integral area was proposed and then verified by measuring the absorption spectra of CO_2 and CH_4 standard gases under various pressures and temperatures. Various measuring gases can avoid the contingency of nonlinearity. The relationship between concentration and integral area was fitted using the new equation, with an average fitting correlation coefficient of 0.9998. The experimental results also demonstrate that the effective optical path length indeed decreases with increasing concentration,

which is a key factor that often causes nonlinear phenomena between signals and concentrations. Furthermore, the cavity reflectances (99.99644% at 6242.6 cm^{-1} and 99.99833% at 6046.96 cm^{-1}) derived from the fitting coefficient of the new concentration expression closely match the reflectances (99.99727% at 6242.6 cm^{-1} and 99.99868% at 6046.96 cm^{-1}) obtained by applying the classical formula to the spectra of the lowest gas concentration. This result further validates the accuracy of the newly proposed concentration expression. These experimental results validate the theoretical deduction process and formula, providing valuable insights for the future development and practical application of OA-ICOS. This work is of great significance for advancing high-precision trace gas detection technology.

Acknowledgements

Project supported by the National Natural Science Foundation of China (Grant Nos. 62005108 and 62205134), Xuzhou Science and Technology Plan Project (Grant No. KC23078), and the Research and Innovation Plan for Graduate Students in Jiangsu Province, China (Grant Nos. KYCX25_3165 and KYCX24_3016).

References

[1] Wang K, Shao L, Chen J, Wang G, Liu K, Tan T, Mei J, Chen W and Gao X 2020 *Sensors* **20** 6192

[2] Yu R, Xia H, Pang T, Wu B, Li Z, Sun P, Guo Q, Zhang Z and Cai Y 2023 *Opt. Commun.* **545** 129731

[3] Shao L, Mei J, Chen J, Tan T, Wang G, Liu K and Gao X 2023 *Microw. Opt. Technol. Lett.* **65** 1489

[4] Yang N, Fang B, Wang C, Zhou H, Wei N, Zhao W and Zhang W 2023 *Acta Photon. Sin.* **52** 0352123

[5] Nadeem F, Mandon J, Cristescu S M and Harren F J M 2018 *Appl. Opt.* **57** 8536

[6] Engel G S, Moyer E J, Keutsch F N and Anderson J G 2001 *Proceedings of the NASA Earth Science Technology Conference (ESTC)* (College Park, MD, USA) pp. 28–30

[7] Clouser B W, Sarkozy L and Moyer E J 2018 *Appl. Opt.* **57** 6252

[8] Zheng K, Zheng C, He Q, Yao D, Hu L, Zhang Y, Wang Y and Tittel F K 2018 *Opt. Express* **26** 26205

[9] Wang K 2021 *In-situ Measurement of CO_2 and CH_4 in Atmosphere Using Off-axis Integrated Cavity Spectroscopy*, Ph. D. dissertation (Hefei: University of Science and Technology of China) (in Chinese)

[10] Han L 2018 *Research on ^{13}C, ^{18}O isotopes in CO_2 measurement technology based on off-axis integrated cavity output spectroscopy*, Ph. D. dissertation (Hefei: University of Science and Technology of China) (in Chinese)

[11] Ko K H, Kim Y, Kim T S, Lee L and Park H 2022 *Appl. Phys. B* **128** 149

[12] Tian X 2019 *Research on High Sensitivity Spectral Detection Technology for Trace Components in Natural Gas*, Ph. D. dissertation (Hefei: University of Science and Technology of China) (in Chinese)

[13] Wang J 2019 In-situ Measurement of Dissolved Gases in Water Using Off-axis Integrated Cavity Spectroscopy, Ph. D. dissertation (Hefei: University of Science and Technology of China) (in Chinese)

[14] Wang Y, Ding B, Wang K, Mei J, Han Z, Tan T and Gao X 2022 *Chin. Phys. B* **31** 040705

[15] Oshina I and Spigulis J 2021 *Journal of Biomedical Optics* **26** 100901

[16] Li P, Lin G, Chen J and Wang J 2024 *Sensors* **24** 5226

[17] Yang C, Wen M, Chen C, Li C, Huang J, Song L and Li Y 2025 *Appl. Sci.* **15** 5562